Draft version May 10, 2016
Preprint typeset using LaTeX style emulateapj v. 5/2/11

arXiv:1605.02194v1 [astro-ph.GA] 7 May 2016

THE HOST GALAXY PROPERTIES OF VARIABILITY SELECTED AGN IN THE PAN-STARRS1 MEDIUM-DEEP SURVEY

S. Heinis[1], S. Gezari[1], S. Kumar[1], W. S. Burgett[2], H. Flewelling[2], M. E. Huber[2], N. Kaiser[2], R. J. Wainscoat[2],C. Waters[2]

Draft version May 10, 2016

ABSTRACT

We study the properties of 975 active galactic nuclei (AGN) selected by variability in the Pan-STARRS1 Medium-Deep Survey. Using complementary multi wavelength data from the ultraviolet to the far-infrared, we use SED fitting to determine the AGN and host properties at $z < 1$, and compare to a well-matched control sample. We confirm the trend previously observed that the variability amplitude decreases with AGN luminosity, but on the other hand, we observe that the slope of this relation steepens with wavelength resulting in a "redder when brighter" trend at low luminosities. Our results show that AGN are hosted by more massive hosts than control sample galaxies, while the restframe, dust-corrected $NUV - r$ color distribution of AGN hosts is similar to control galaxies. We find a positive correlation between the AGN luminosity and star formation rate (SFR), independent of redshift. AGN hosts populate the whole range of SFRs within and outside the Main Sequence of star forming galaxies. Comparing the distribution of AGN hosts and control galaxies, we show that AGN hosts are less likely to be hosted by quiescent galaxies, but more likely to be hosted by Main Sequence or starburst galaxies.

Subject headings: galaxies: nuclei–galaxies: star formation

1. INTRODUCTION

One of the remaining class of puzzling astronomical objects is active galactic nuclei (AGN). AGN emission is powered by massive black holes, which are expected to be hosted by most massive galaxies (Magorrian et al. 1998) and virtually all galaxies. Besides the interest in high energy physics and strong gravity involved in the processes shaping their emission, AGN are also crucial in the context of galaxy formation and evolution. The energy released by AGN in the interstellar medium has long been invoked by simulation studies to explain the quenching of star formation activity in massive galaxies (e.g. Croton et al. 2006). Evidence for active feedback has also been brought by observations (e.g. Fabian 2012; Tombesi et al. 2015), but remains highly controversial. Indeed while a number of studies found that AGN activity seems to shut down star formation (e.g. Schawinski et al. 2009; Farrah et al. 2012; Page et al. 2012), similar number of studies show that they do not (e.g. Netzer 2009; Mullaney et al. 2012a; Rosario et al. 2013), and that on the other hand AGN luminosity is positively correlated with star formation rate (Mullaney et al. 2012b), while this relation has also been observed to be flat in redshift intervals at $z < 2.5$ (Stanley et al. 2015).

Over the last decade, there has also been considerable work on understanding the triggering mechanisms of the AGN activity. The most common scenario is that gas-rich galaxy mergers trigger AGN activity, which in turn quenches star formation (Hopkins et al. 2008). Observations do not fully support this scenario however: while luminous quasar hosts display signatures of current or past merger activity (Stockton 1982; Canalizo & Stockton 2001; Bennert et al. 2008) moderate luminosity AGN on the other hand reside preferentially in galaxies displaying undisturbed morphologies (Gabor et al. 2009; Cisternas et al. 2011; Kocevski et al. 2012).

Most of the aforementioned studies focused on AGN selected from their X ray emission or ultraviolet/optical emission lines. While successful, these studies are biased against heavily obscured AGN (which can be detected in the far-infrared), and low luminosity AGN, where the contribution of the host galaxy can be of the same order or larger than that of the AGN. With the advent of large time domain surveys such as Pan-STARRS1 (Kaiser et al. 2010), and the upcoming LSST (Ivezic et al. 2008), a new window is opening for building large samples of AGN using variability as a complementary selection (e.g. Sarajedini et al. 2006; Schmidt et al. 2010; Sesar et al. 2007; Villforth et al. 2012) albeit with its own set of selection biases, including a bias against Type 2 AGN. Indeed, AGN display variability over the whole spectrum and over a wide range of timescales, which is thought to be related to accretion disk instabilities, while long term variability for the so-called "changing-look quasars" explained by variable obscuration (e.g. Cohen et al. 1986; Denney et al. 2014; Tohline & Osterbrock 1976; Shappee et al. 2014) or change in the ionizing flux of the central source itself (LaMassa et al. 2015) has been observed only in a handful of objects.

Variability selection enables one to probe a large range of AGN luminosities, and is not biased against low luminosity objects, as the amplitude of AGN variability actually increases for fainter AGN (e.g. Hook et al. 1994; Trevese et al. 1994; Vanden Berk et al. 2004; Wilhite et al. 2008; Bauer et al. 2009; Zuo et al. 2012; Gallastegui-Aizpun & Sarajedini 2014). In this paper, we revisit the connection between AGN and host galaxy properties, using a sample of $\sim$ 1000 AGN selected by their optical variability in the Pan-STARRS1 Medium Deep Survey, and com-

[1] Department of Astronomy, University of Maryland, College Park, MD, USA
[2] Institute for Astronomy, University of Hawaii at Manoa, Honolulu, HI 96822, USA

plemented by ancillary data from the ultraviolet (UV) to the far-infrared (FIR). Thanks to this large wavelength coverage, we are able to separate the AGN and the host contributions to the observed SED, in order to investigate the link between host and AGN properties. While large samples of point-like quasars have previously been built through variability selection (e.g. MacLeod et al. 2012), only small sets (~ 50) have been considered to investigate the AGN-host properties connection (Villforth et al. 2012; Klesman & Sarajedini 2014).

This paper is organized as follows: in §2 we present our variability selected AGN sample, as well as the ancillary data. §3 describes our fitting method to separate the AGN and host contribution to the obvserved SED. In §4 we present our results, which are further discussed in §5, before concluding in §6. Throughout we use a $\Lambda-$flat cosmology ($\Omega_M = 0.3$, $\Omega_\Lambda = 0.7$, $H_0 = 70\,\mathrm{km.s^{-1}.Mpc^{-1}}$), and a Chabrier (2003) initial mass function (IMF).

2. DATA

2.1. *Variability selected AGN*

We use the sample of candidate AGN selected by variability from Kumar et al. (2015). We only recall here the main characteristics of the method. We refer the reader to Kumar et al. (2015) for full details. Our sample is based on the classification of extragalactic variable sources detected during the first 2.5 years of PS1 observations. During their $\sim$ 5 month window of seasonal visibility, each PS1 Medium Deep Field is observed nightly, cycling through 4 filters (Tonry et al. 2012) ($g_{\rm PS1}(\lambda_{\rm eff} = 481$ nm), $r_{\rm PS1}(\lambda_{\rm eff} = 617)$ nm), $i_{\rm PS1}(\lambda_{\rm eff} = 752)$ nm), and $z_{\rm PS1}$ ($\lambda_{\rm eff} = 866$) nm), with observations in the same filter every 3 nights, and observations in the $y_{\rm PS1}$ ($\lambda_{\rm eff} = 962$) nm) filter near the full moon, with an average number of total epochs per filter for this 2.5 year sample of 36. Nightly images are processed through a frame subtraction analysis pipeline, and sources are tagged as a transient and published to an alerts database if they are detected with a signal-to-noise (S/N) ≥ 5 in at least 3 difference images within a time window of 15 days. While this pipeline was designed to detect supernovae, variability in the nuclei of galaxies also is detected as positive and negative excursions in the difference images. We then match these transient alerts with a catalog created from the stacked PS1 images (described in §2.2), and only classify the light curves of transients within the Kron elliptical radius of an extended galaxy with $i < 24$ mag, the magnitude range for which the star/galaxy classification is reliable.

The light curves of variable sources in $g_{PS1}, r_{PS1}, i_{PS1}$, and z_{PS1} image differencing are fitted with five models: a Gamma distribution, a Gaussian distribution, an analytic supernova (SN) model (all three modeling SN-like lightcurves); an Ornstein−Uhlenbeck (OU) process (modeling AGN-like lightcurves, Kelly et al. 2009); and a constant flux model (modeling noise). The quality of the fits is then used to classify the variable sources using a K-means clustering algorithm with 3 centers (SN, AGN, or noise model). Out of 4361 extragalactic transient alerts, the light curves of 2262 are classified as similar to those of AGN and considered "nuclear". We further restrict the sample to objects with $i_{\rm PS1} > 18$, in order to avoid bright galaxies, where the difference imaging is more likely to introduce image differencing artifacts that can cause centroid errors and false nuclear positive. This cut minimizes the contamination of by non-AGN to 16%, according to a verification set of objects with spectroscopic redshifts, while maximizing the number of AGN in the sample. We are then left with 1768 objects.

2.2. *Pan-STARRS1 data*

We perform our custom reduction of the Pan-STARRS1 Medium Deep data survey. We use the stacks generated by the Pan-STARRS1 image processing pipeline (Magnier 2006), and also the CFHT u band data obtained by E. Magnier as follow up of the Medium Deep fields, which covers 65 % of the survey. We have at hand 6 bands: $u_{\rm CFHT}$, $g_{\rm PS1}$, $r_{\rm PS1}$, $i_{\rm PS1}$, $z_{\rm PS1}$, and $y_{\rm PS1}$. We perform photometry using the following steps; we consider the Pan-STARRS1*skycell* as the smallest entity: *i)* resample the u band images to the Pan-STARRS1 resolution ($0.25''$per pixel), and register all images; *ii)* for each band fit the PSF to a Moffat function, and match that PSF to the worse PSF in each skycell; *iii)* using these PSF-matched images, we derive a χ^2 image (Szalay et al. 1999); *iv)* we perform photometry using the dual mode of SExtractor (Bertin & Arnouts 1996), detecting objects in the χ^2 image and measuring the fluxes in the PSF matched images: the Kron-like apertures are defined from the χ^2 image and hence are the same over all bands. The detection threshold, defined by the χ^2 distribution, is equivalent to a signal-to-noise ratio (SNR) of 1.9σ.

2.3. *Other datasets*

We cross match our AGN sample to a number of other datasets to constrain their SEDs.

2.3.1. *GALEX*

We first cross match our sample with the public GALEX (Martin et al. 2005) data[3] using a $5''$ radius using by decreasing order of priority: data from the Deep Imaging Survey (DIS), the Medium Imaging Survey (MIS), and the All-sky Imaging Survey (AIS). For the DIS, we use the standard pipeline data, while for the MIS and the AIS, we use the GCAT Unique Source Catalogs[4], which contains the standard pipeline photometry, as well as optimized photometry for extended objects ($< 1'$). 83% of sources have a GALEX cross match. Budavári et al. (2009) and Seibert et al. (2005) show that $5''$is the optimal search radius for GALEX-SDSS matches, and estimate an upper limit of 2% for the number of false matches.

We make then use of the University of Maryland Time Domain Survey data (Gezari et al. 2013, 2015). We remeasure the GALEX photometry for objects which are in images where the exposure time (in FUV or NUV) is greater than the archive images. We also derive an upper limit at 1σ for non detected sources. This process adds photometry for 7% sources. Finally, we also attempt to measure the photometry for all objects without a cross match with GALEX archive data, or derive an upper limit if no detection is found.

[3] `http://galex.stsci.edu/casjobs/`
[4] `http://archive.stsci.edu/prepds/gcat/`

2.3.2. *Spitzer*

We cross match our sample with the Spitzer Enhanced Imaging Products (SEIP)[5] using a 2″search radius. 95% of our sources have a match within 1″. According to the SWIRE release 2[6], we expect only a few percents of false positive matches in that range.

The SEIP contains high quality photometry in IRAC (3.6, 4.5, 5.8, and 8. μm), and MIPS (24 μm) bands. 54% of objects in our sample have a cross match with SEIP sources.

2.3.3. *WISE*

We cross match our sample with the custom reduction of the WISE data from Lang et al. (2014, unWISE) using a cross match search radius of 1″. Lang et al. (2014) performed prior photometry based on SDSS sources in their own version of the WISE coadds (Lang 2014). This version of the WISE catalog has the advantage to provide a WISE flux for all SDSS sources, at the SDSS angular resolution. We find a cross match for 93% of objects; given the fact that unWISE is based on SDSS prior positions, we expect a few percents of false positive matches.

2.3.4. *Spectroscopic redshifts*

We cross match our sample with a number of spectroscopic catalogs,using a search radius of 1″. We expect only a few percents of false matches as all these datasets are based on optical data. We cross match with SDSS DR12 (Alam et al. 2015), which provides most of the spectroscopic counterparts. We also cross match with the following surveys: the COSMOS bright spectroscopic sample (Lilly et al. 2007), the PRIMUS survey (Coil et al. 2011; Cool et al. 2013), the VIPERS survey (Guzzo et al. 2014), the VVDS survey (Le Fèvre et al. 2004, 2005; Garilli et al. 2008), the DEEP2 survey (Newman et al. 2013), and the Veroncat catalogue (Véron-Cetty & Véron 2010). Among our 1768 objects, 585 (33%) have a spectroscopic redshift, 493 (85% of the spectroscopic objects) have been classified as AGN, and 87 (15%) as galaxies.

2.4. *Photometric redshifts*

We estimate photometric redshifts using the code `lephare` (Arnouts et al. 1999; Ilbert et al. 2006). `lephare` determines photometric redshifts by fitting the observed photometry to libraries of galaxies, quasars, and stars template SEDs. We use our training set built from objects with spectroscopic redshifts to assess the quality of the photometric redshifts. We do not include here Spitzer 24 μm as well as the $W3$ and $W4$ WISE bands, as they probe ranges of the SED not dominated by stellar emission in the redshift range we are interested in. Determining photometric redshifts with small errors for AGN/quasar dominated objects is notoriously difficult, as the SEDs of these objects are close to featureless (see e.g. Richards et al. 2009), and narrow band photometry is required to improve significantly the quality of the estimates (Salvato et al. 2011).

[5] `http://irsa.ipac.caltech.edu/data/SPITZER/Enhanced/SEIP/overview.html`

[6] `http://irsa.ipac.caltech.edu/data/SPITZER/SWIRE/docs/delivery_doc_r2_v2.pdf`

We performed extensive tests in order to obtain the best photometric redshifts for our AGN sample. We first determine the zero point offsets for the bands. We compared the flux from best fitting galaxy SED models for spectroscopic galaxies in our sample to the actual photometry (Ilbert et al. 2009). In a second step, we tested a number of combinations for the AGN-dominated SED templates. We obtain the best results by using a subset of 22 templates out of the 30 templates used by Salvato et al. (2009). We trimmed the list of 30 templates by excluding the templates which are never retained as best model when the fitting is performed with the redshift fixed at its spectroscopic value.

We show a comparison of the photometric and spectroscopic redshifts on Fig. 1. Using $\Delta z = z_{\rm spec} - z_{\rm phot}$, we quantify the error on the photometric redshifts as $err(z) = \Delta z/(1+z_{\rm spec})$, and use as a global measure the normalized median absolute deviation $\sigma_{\Delta z/(1+z_{\rm spec})} = 1.4826 * {\rm median}(|err(z) - {\rm median}(err(z))|)$. We consider as outliers objects with $|err(z)| > 0.15$, and note the percentage of these objects as η. For our full spectroscopic sample, the overall error is $\sigma_{\Delta z/(1+z_{\rm spec})} = 0.08$, and $\eta = 28.1\%$. These numbers are in agreement with those usually obtained using broadband photometry (e.g. Salvato et al. 2011).

For this study, we chose hereafter to restrict the sample to objects with $0.1 < z_{\rm phot} < 1$; these limits are shown as dotted lines on Fig. 1. We ensure the upper limit as the quality of the photometric redshifts decreases significantly for $z > 1$, and the lower limit in order to avoid outliers a low redshifts. In this range, the error is $\sigma_{\Delta z/(1+z_{\rm spec})} = 0.06$, and $\eta = 17.5\%$. Our final cuts leave us with 1160 objects. We further use spectroscopic redshifts whenever available. Doing so lowers the actual errors on photometric redshifts in our sample. In order to derive the resulting errors, we assume that the redshift errors for objects with spectroscopic redshifts are negligible compared to the photometric redshift errors. Assuming objects without spectroscopic redshifts (757 objects) have the same photometric redshift errors than those with spectroscopic redshifts (403 objects), the actual error for our final AGN sample is $\sigma_{\Delta z/(1+z_{\rm spec})} = 0.03$, and the percentage of outliers $\eta = 11.5\%$.

2.5. *Control sample*

We build a control sample from the full catalogue from one of the Medium Deep fields, MD04. We first follow the same procedure as for the AGN sample described above to obtain photometry in other wavelengths (see Sect. 2.3). We use only extended objects following our custom star/galaxy separation, based on machine learning techniques (Heinis et al., submitted). We determine photometric redshifts using the code `lephare`. The error on photometric redshifts is $\sigma_{\Delta z/(1+z_{\rm spec})} = 0.05$ and the outliers percentage $\eta = 11\%$. We keep objects with the same distribution in $i_{\rm PS1}$ than the AGN sample. We also limit the sample to $0.1 < z_{\rm phot} < 1.$, as for the AGN sample. We are left with 16,401 objects.

3. SED FITTING

3.1. *pCIGALE*

Table 1
Statistics of available photometry

	FUV	NUV	u	$g_{\rm PS1}$	$r_{\rm PS1}$	$i_{\rm PS1}$	$z_{\rm PS1}$	$y_{\rm PS1}$	i_1	i_2	i_3	i_4	m_1	W_1	W_2	W_3	W_4
% detections	74	86	80	100	100	100	100	100	50	50	45	46	36	93	93	82	67
% upper limits	9	5	0	0	0	0	0	0	0	0	1	1	9	0	0	0	0

Statistics of available photometry for the AGN sample. For each band, we give the percentage of objects with detections, and the percentage of objects with upper limits.

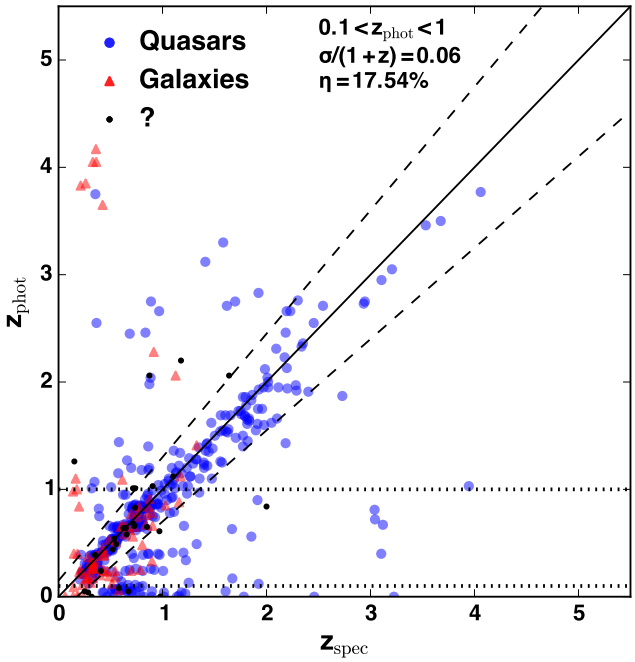

Figure 1. Photometric redshifts vs spectroscopic redshifts for the AGN sample. Blue circles represent spectroscopic quasars, red triangles spectroscopic galaxies, and black dots spectroscopic objects without classification available. The solid line shows $z_{\rm spec} = z_{\rm phot}$, while the dashed lines correspond to $|z_{\rm spec} - z_{\rm phot}|/(1 + z_{\rm spec}) = 0.15$. The dotted lines show our chosen cuts in $z_{\rm phot}$.

We use the code `pCIGALE`[7] to perform SED fitting and estimate physical parameters. `pCIGALE` is `python` version of the former `CIGALE` code (Noll et al. 2009), which besides the different coding language, also provides new features. `pCIGALE` preserves the same features of `CIGALE`, however this new version has been designed for a broader set of scientific applications as well as improved performance. We provide here a short description of the latest version of `pCIGALE` to date.

`pCIGALE` (see also Ciesla et al. 2015) has two different and independent functions: SED modeling (Boquien et al., in prep.) and SED fitting (Burgarella et al, in prep.). The SED modeling function allows one to build a galaxy SED from the UV to the sub-mm based on single stellar population synthesis models, chosen star formation histories (SFHs), and energy balance. The full SED is built by re-emitting in the IR the energy absorbed by dust in the UV-optical. We use here delayed star formation histories, which have been shown to reproduce accurately the SEDs of galaxies over a wide redshift range:

$$\mathrm{SFR}(t) = (t - t_{\rm age}) \exp\left(\frac{t - t_{\rm age}}{\tau_{\rm main}}\right) \qquad (1)$$

[7] `http://cigale.lam.fr/`

We consider the stellar population models of Bruzual & Charlot (2003), which are convolved by the SFH, and then attenuated by dust. We use the law of Calzetti et al. (2000) to estimate the extinction by dust, and the librairies of Dale et al. (2014) to model the re-emission in the IR of this energy. Using `pCIGALE`, Buat et al. (2014) showed that the constraint from the IR restframe range is essential to derive accurate SFR estimates. In particular they found that SFR estimated by SED fitting without IR data are on average overestimated by 20%. In details, low SFR are overestimated and large SED are underestimated, by factors up to 2.5. They also showed that the intrinsic dispersion in SFR increases by a factor 2 when no IR data is used.

Finally, `pCIGALE` also allows us to include AGN emission, to be added to the stellar one, using the templates from Fritz et al. (2006). The Fritz et al. (2006) templates consist of two components: the central source and dust. The emission of the central source is assumed to follow power laws with a different index in three wavelength ranges (spanning $0.001 < \lambda < 20\mu$m). The dust component consists of scattering and the thermal emission from the absorbtion in the UV/optical. The dust torus itself is modeled using a flared disc geometry (Efstathiou & Rowan-Robinson 1995). The models of Fritz et al. (2006) have been extensively tested in previous work (e.g. Hatziminaoglou et al. 2008, 2010; Feltre et al. 2012). We list in Table 2 the parameters we use for the SED fitting.

`pCIGALE` creates a library of models combining all parameters; for each model, a number of properties are derived, such as the stellar mass (M_*), the star formation rate averaged over the last 100 Myr etc. For the AGN component, we compute for each model the luminosity at 5100 Å (L_{5100}), as well as the absolute magnitude in the $g_{\rm PS1}$ band. `pCIGALE` computes the χ^2 statistics for each model, and builds the probability distribution function (PDF) for each parameter and derived property using these χ^2 values. The parameter or property value we use is the average value weighted over this PDF and the error the standard deviation which thus encodes the width of this PDF. In the following, we use only objects with $\chi^2_{\rm reduced} < 5$ (975 objects).

Ciesla et al. (2015) in particular tested the performance of `pCIGALE` to recover the properties of AGNs in the case of realistic SFHs drawn from a semi-analytic simulation. Ciesla et al. (2015) show that `pCIGALE` is able to recover accurately both the properties of the AGNs and the host galaxy, provided that the observed SED is constrained from the UV to the FIR restframe, and also that the fraction of the AGN emission in the IR, $f_{\rm AGN}$ is larger than 0.1.

3.2. *AGN luminosity: SEDs vs spectra*

Table 2
pCIGALE fitting parameters

Parameter	Value	Description
	Delayed Star Formation History	
$\tau_{\rm main}$[Myr]	10.,50.,100.,500.,1000.,5000.,10000.,100000.	Star formation timescale
age [Myr]	100.,1000.,5000.,7000.,9000.,11000.,13000.,13536.	Age of the oldest stars inthe galaxy
	Extinction law (Calzetti et al. 2000)	
$E(B-V)$	0.01,0.05,0.1,0.2,0.3,0.5	Color excess of the stellar continuum
	Dust templates (Dale et al. 2014)	
$\alpha_{\rm SF}$	1,2,3,4	Exponent of the intensity of the radiation field
	AGN models (Fritz et al. 2006)	
$R_{\rm max}/R_{\rm min}$	60	Ratio of the external to internal radius of the dust torus
$\tau_{\rm dust}$	0.1,0.6,2.0,6.0,10.	Optical depth at 9.7μm of the dust torus
β	-0.5	Parameter describing the torus density profile
γ	4.	Parameter describing the torus density profile
Θ [deg]	40.	Opening angle of the dust torus
ψ [deg]	89.99 (Type 1)	Angle between the AGN axis and the line of sight
$f_{\rm AGN}$	0.05,0.1,0.15,0.2,0.25,0.3,0.35,0.4,0.45,0.5,0.55,0.6,0.65,0.7	AGN fraction in the IR

Parameters used for the SED fitting with pCIGALE. For the templates of Dale et al. (2014), we fix the AGN fraction to 0.

One of the main AGN properties we will use hereafter is the luminosity at 5100 Å, L_{5100}. Using a spectroscopic sample, we check how well we can recover L_{5100}. We use all the objects in our sample with a counterpart in SDSS DR12 having a spectrum classified as a quasar. We correct the spectra for Galactic extinction using the Schlegel et al. (1998) map, and the extinction curve from Cardelli et al. (1989), with $R_V = 3.1$; we also shift the spectra to restframe using the listed redshift. We are only interested here in the continuum luminosity, so we fit the continuum with a power law ($L_\lambda = A\lambda^\alpha$) for $2500 < \lambda[\AA] < 5500$, and exluding the regions of the spectra around the Mg II, Hβ, and O III lines. We then obtain the luminosity at 5100 Å as λL_λ. This measure can be contaminated by the host luminosity, so we use eq. 1 from Shen et al. (2011) to correct our estimate from host contribution. On the other hand, we fit the broadband photometry SED of the same objects with pCIGALE. We compare the luminosities at 5100 Å we derive from the SED and the spectra in Fig. 2.

In Fig. 2, we show the results of the SED fitting using AGN of Type 1, as among our objects with spectroscopic redshifts and classifications, only 5% are Type 2. As can be seen in Fig. 2, there is excellent agreement between the two methods.

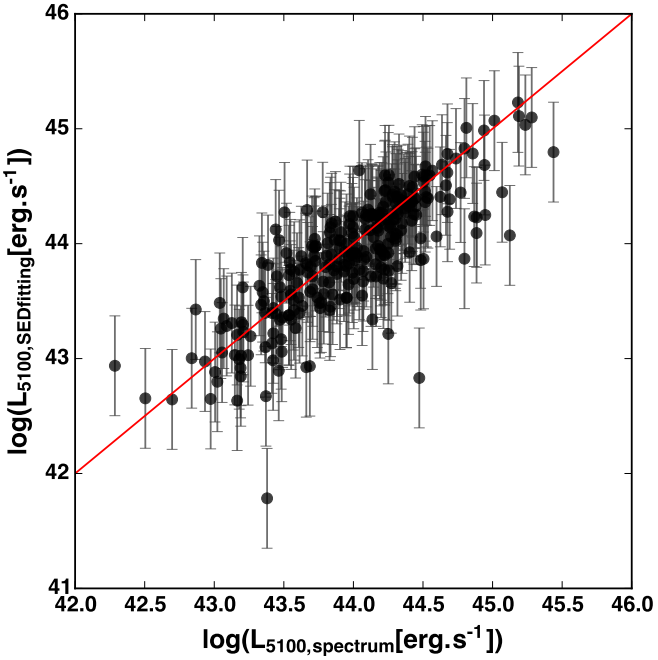

Figure 2. Comparison of SED fitting measurement of L_{5100} with measurement from spectra. We compare the estimate of L_{5100} obtained from pCIGALE(y-axis) with the one obtained directly from the spectrum (x-axis).

4. RESULTS

4.1. *Stellar Mass Distribution*

In Fig. 3 we show the stellar mass distribution of the AGN derived by pCIGALE (blue shaded histogram). We compare it with that of the control sample (gray shaded histogram). Fig 3 suggests that the stellar mass distribution of AGNs is different from inactive galaxies: it is skewed towards large masses ($\sim 10^{10.6} M_\odot$). We checked whether the variability selection can explain this trend, by simulating the level of variability for galaxies in our control sample. We assume that each galaxy in the control sample hosts an AGN, and assign a black hole mass $M_{\rm BH}$ using the total stellar mass - black hole mass relation from Bennert et al. (2011). We then convert $M_{\rm BH}$ to Eddington luminosity, and further to a bolometric luminosity using the Eddington ratio distribution from Kelly et al. (2010). Using the bolometric correction of Krawczyk et al. (2013), we obtain an estimate of L_{5100}. We assume that the AGN have a power law SED $f_\lambda \propto \lambda^{-1.5}$, and use this luminosity as normalization. We derive the AGN flux in the PS1 g filter, and finally use the relation we observe between the fractional variability $\Delta f/f$ and L_{5100} (see Sect. 4.3). We compute what the

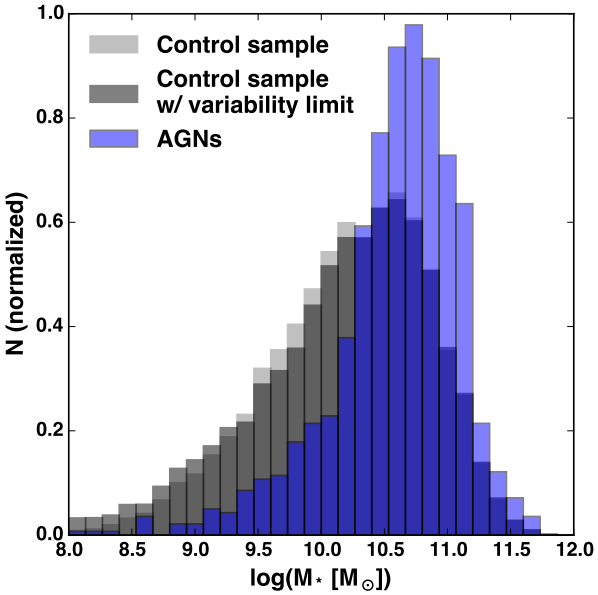

Figure 3. Stellar mass distribution. The blue shaded histogram shows the stellar mass distribution of the AGN sample. The gray shaded histogram shows the distribution of the full control sample, and the black shaded histogram the distribution of the control sample with an additional cut imposed on simulated variability.

brightest magnitude $min_{\rm g}$ is for this simulated variable source, and keep only objects with $min_{\rm g} < 23$ mag (the sentivity limit for the detection of sources in the PS1 difference imaging). The resulting stellar mass distribution is shown in shaded black in Fig. 3. It is clear that the variability cut has little impact on the control sample stellar mass distribution. This is expected as the AGN luminosity is correlated with the host stellar mass (given the black hole mass-stellar mass correlation, e.g. Häring & Rix 2004; Kormendy & Ho 2013; McConnell & Ma 2013; Reines & Volonteri 2015), but anti-correlated with the amplitude of variability.

Thus the results presented in Fig. 3 suggest that AGN are mostly hosted by larger stellar mass galaxies than the underlying galaxy population.

4.2. *Color Distribution*

We show in Fig. 4 (left panel) the distribution of the total restframe $NUV - r$ color, i.e. the combination of the host and AGN. Note that this color is corrected for dust attenuation. Given the different mass distributions of the control sample and the AGN, we use here a mass-matched version of the control sample. We show as dashed lines on Fig. 4 the limits of the Green Valley (e.g. Wyder et al. 2007). As expected, compared to the control sample, the distribution of AGN host total colors peaks in the blue sequence, as the AGN emission contributes significantly to the SED, and can dominate over the stellar populations. In the right panel, we show the distribution of the host galaxy only restframe $NUV - r$ color, given by our SED fitting decomposition. Here the distribution of the host colors is strikingly similar to that of the control sample. In other words, our results show that hosts of AGN have the same color distribution than regular, non-AGN galaxies. There is no obvious link between harboring an AGN and the restrame $NUV - r$ color of its host galaxy stellar population.

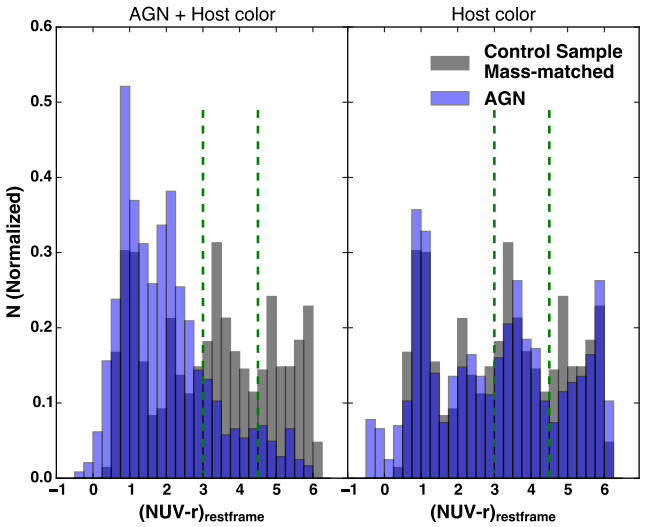

Figure 4. $(NUV - r)_{\rm restframe}$ distribution. The gray shaded histograms show the distribution of the mass-matched control sample, while the blue shaded histograms show the distribution of the AGN sample. Left panel shows the distribution of the total $(NUV - r)_{\rm restframe}$ color for the AGN (i.e. including both the AGN and the host). Right panel shows the distribution of the host color only for the AGN sample. On both panels, the vertical dash lines show the limits for the Green Valley.

4.3. *Amplitude of variability*

We investigate the relation between the amplitude of the AGN variability and the AGN luminosity. We use the measure from the image differencing of the minimum magnitude in the g, r, i, and z bands, i.e. the maximum flux of the variable component of the AGN measured over the course of the survey. We convert this magnitude to an absolute magnitude, e.g. $M_{g,\rm min}$ and derive the relative amplitude of the variability as

$$\log\left(\frac{\Delta f}{f}_{\rm g}\right) = -0.4(M_{g,\rm min} - M_g) \qquad (2)$$

where M_g is the g-band absolute magnitude of the AGN component derived from the SED fitting, and proceed similarly for the other bands. We derive the AGN bolometric luminosity, $L_{\rm AGN}$, using the relation from Netzer & Trakhtenbrot (2014) for the bolometric correction at 5100 Å: $b_{5100} = 53 - \log L_{5100}$.

We show in Fig. 5 the relation between this measure of variability in the g, r, i, z bands and $L_{\rm AGN}$. We use here only objects (831) that have a measure of the minimum apparent magnitude in g, r, i, z bands. We adjust the relations between $\Delta f/f$ and $L_{\rm AGN}$ by:

$$\log\left(\frac{\Delta f}{f}\right) = \beta\,[\log(L_{\rm AGN}) - 44.5] + \log\left(\frac{\Delta f}{f}\right)_0 \qquad (3)$$

We use Orthogonal Distance Regression to perform these fits. This method allows to take into account errors both on $\frac{\Delta f}{f}$ and $L_{\rm AGN}$. The errors on the parameters for these fits that we quote are the standard errors on the estimated parameters, which are derived from the covariance matrix estimated during the fit. We list in table 3 the best fit parameters in the g, r, i, and z bands.

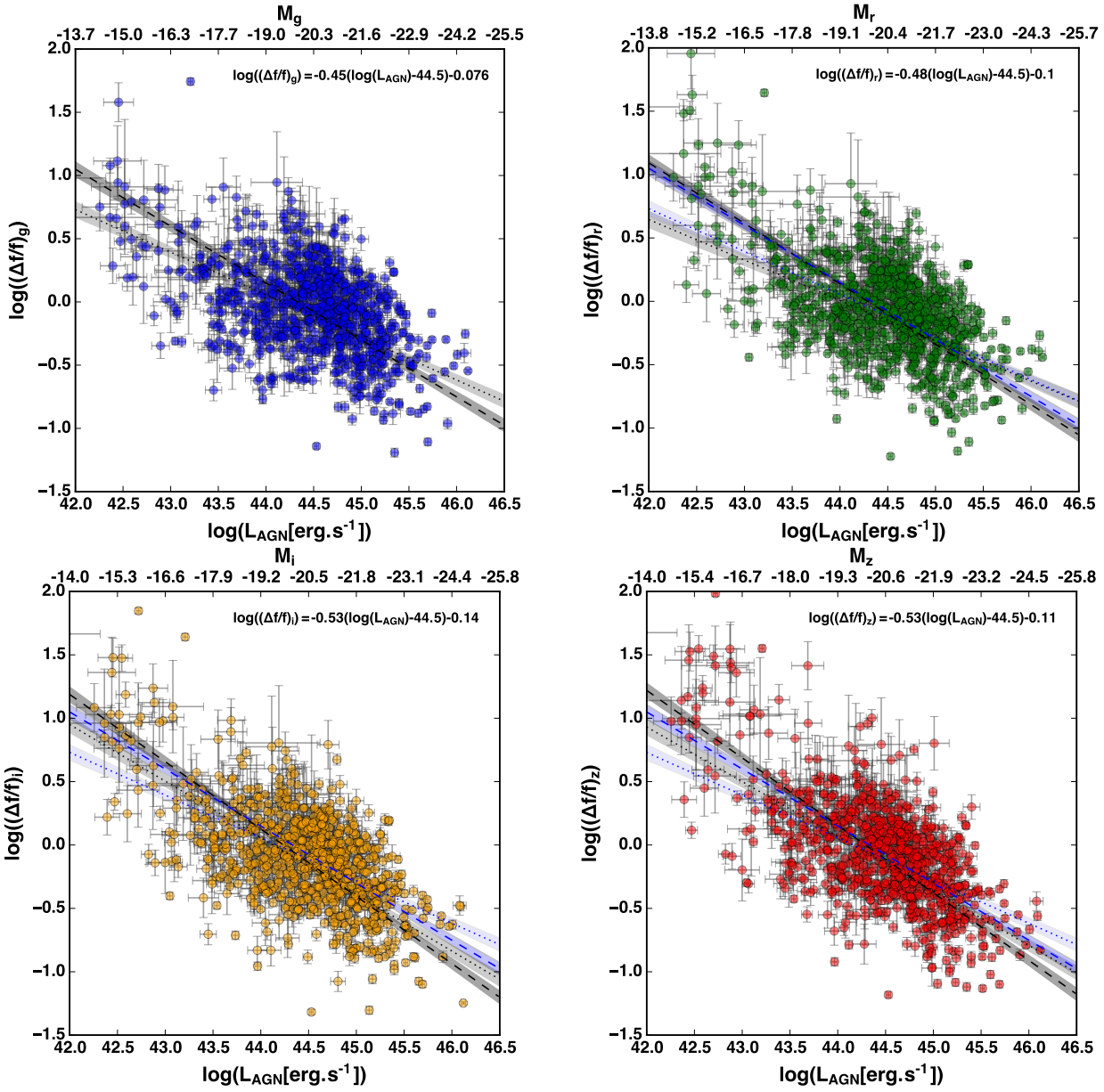

Figure 5. Relative variability amplitude in the g, r, i, and z bands as a function of AGN bolometric luminosity. The upper x-axis shows the corresponding AGN absolute magnitude. In each panel, we show the best fit to eq. 3 as a black dashed line, and the dashed area around it represents the errors on the fit. Similarly, we also show the fit to eq. 3 using only objects with $L_{\rm AGN} > 10^{43.5}$ erg.s^{-1} as a dotted line. On the panels representing the results for the r, i, and z bands, we show in blue the fits obtained in the g band as reference.

Table 3
Best fit parameter values for eq. 3 in the g, r, i, and z bands.

	All objects		$L_{\rm AGN} > 10^{43.5}$erg.s^{-1}	
Band	β	$\log\left(\frac{\Delta f}{f}\right)_0$	β	$\log\left(\frac{\Delta f}{f}\right)_0$
g	-0.45 ± 0.02	-0.08 ± 0.01	-0.34 ± 0.02	-0.11 ± 0.01
r	-0.48 ± 0.02	-0.10 ± 0.01	-0.32 ± 0.02	-0.15 ± 0.01
i	-0.53 ± 0.02	-0.14 ± 0.01	-0.45 ± 0.02	-0.17 ± 0.01
z	-0.53 ± 0.02	-0.11 ± 0.01	-0.43 ± 0.02	-0.15 ± 0.01

We note that our sensitivity to AGN variability is set by our magnitude limit in the difference images of $m_{\rm lim} \sim 23$ mag. Thus, for a variable AGN, a bright AGN will be detected at smaller fractional variability (Δ f/f) amplitudes than a faint AGN: i.e., the faint AGN in our sample require larger $\Delta f/f$ than the bright AGN in order to be detected. We address this bias directly in our simulation described in Section 4.1 and find that this does NOT bias us against detecting AGNs in low-mass galaxies.

In all bands considered here, the overall trend is that the amplitude of the variability decreases with AGN luminosity. Moreover, this relation is steeper at longer wavelengths. Including all objects in the fit, we find that β decreases from ~ -0.45 in the g band to ~ -0.53 in the z band. This steepening of the relation is however mostly due to the objects fainter than $L_{\rm AGN} < 10^{43.5}$erg.s^{-1}. We also perform the fit excluding these objects, and find that while the decrease in β is less pronounced (-0.34 in g to -0.43 in z), it is still significant.

The trends we observe that variability amplitude decreases with AGN luminosity has been noted by a num-

ber of studies (e.g. Hook et al. 1994; Trevese et al. 1994; Vanden Berk et al. 2004; Wilhite et al. 2008; Bauer et al. 2009; Zuo et al. 2012; Gallastegui-Aizpun & Sarajedini 2014). This trend suggests that AGN variability can be interpreted by Poissonian models. The slope of the variability-luminosity relation $\delta L/L \propto L^{\beta}$ is expected to be $\beta = -0.5$ in that case. When we consider all objects in the fit, we find slopes consistent with Poissonian models in r, i, and z bands, while the slope is shallower in g. When we consider only objects with $L_{\rm AGN} > 10^{43.5}$erg.s^{-1}, we find in all bands shallower slopes than $\beta = -0.5$.

Gallastegui-Aizpun & Sarajedini (2014) also observed that the slope of the variability function steepens between the g, r, and i SDSS bands for Type 1 AGN. We note that Gallastegui-Aizpun & Sarajedini (2014) constrained the variability function down to $M_i \sim -18.5$, while we extend here the range of measurements down to $M_i \sim -14$. Numerous studies (Vanden Berk et al. 2004; Zuo et al. 2012; Gallastegui-Aizpun & Sarajedini 2014) have reported that the amplitude of variability is larger at bluer wavelengths. Thanks to our sample spanning a larger range of bolometric luminosities, we can revisit this claim. At $L_{\rm AGN} \gtrsim 10^{43.5}$erg.s^{-1}, we observe that on average the amplitude of variability is larger in g than in the other bands, which is consistent with previous results. At fainter luminosities however, which were not sampled by previous studies, AGN display larger variability amplitudes in redder bands. We examine in Fig. 6 the wavelength and luminosity dependence of the relative variability amplitude. We show in four bins of $\log(L_{\rm AGN})$ the average relative variability amplitude as a function of restrame wavelength. The errors bars are derived by propagating the errors in the mean. These measures show that for $43 < \log(L_{\rm AGN}[\rm erg.s^{-1}]) < 45$, there is no significant wavelength dependence of the AGN variability (i.e. the relation is consistent with a flat one at the $1\,\sigma$ level). For bright AGNs, at $45 < \log(L_{\rm AGN}[\rm erg.s^{-1}]) < 46.5$, we observe that the variability decreases at redder wavelengths ($2.5\,\sigma$ level), while for faint AGNs, at $42 < \log(L_{\rm AGN})[\rm erg.s^{-1}] < 43$, the trend reverses, as the variability increases at redder wavelengths ($2.7\,\sigma$ level).

4.4. *AGN and host SFR*

We investigate in Fig. 7 the relation between the host SFR and the AGN bolometric luminosity. Our results show that for variability selected AGN, there is an overall good correlation between SFR and the bolometric AGN luminosity. We also color code in Fig. 7 the symbols by the redshifts of the objects. This shows that higher redshift objects display higher SFRs and bolometric AGN luminosity. The observation that the commonly observed SFR-$L_{\rm AGN}$ relation is built from the contribution of galaxies at various redshifts is consistent with the results from Stanley et al. (2015) based on a X-ray selected sample. Stanley et al. (2015) furthermore found that, at a given redshift, there is no correlation between SFR and $L_{\rm AGN}$: At a given redshift ($0.2 < z < 2.5$), the relation between SFR and $L_{\rm AGN}$ is mostly flat, while the amplitude of this relation increases with redshift. The superposition of these relations yields the impression of an overall correlation between SFR and $L_{\rm AGN}$. In contrary to Stanley et al. (2015), the overall relation between SFR

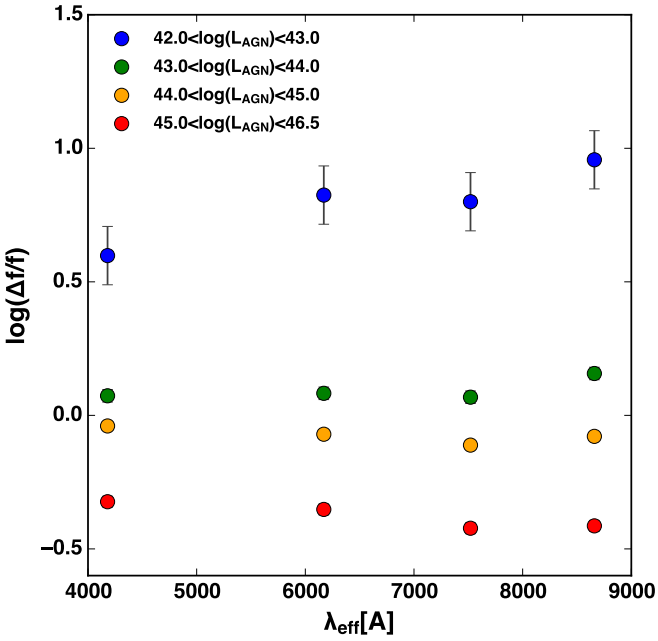

Figure 6. Average relative variability amplitude as a function of restframe wavelength in four bins of AGN luminosity.

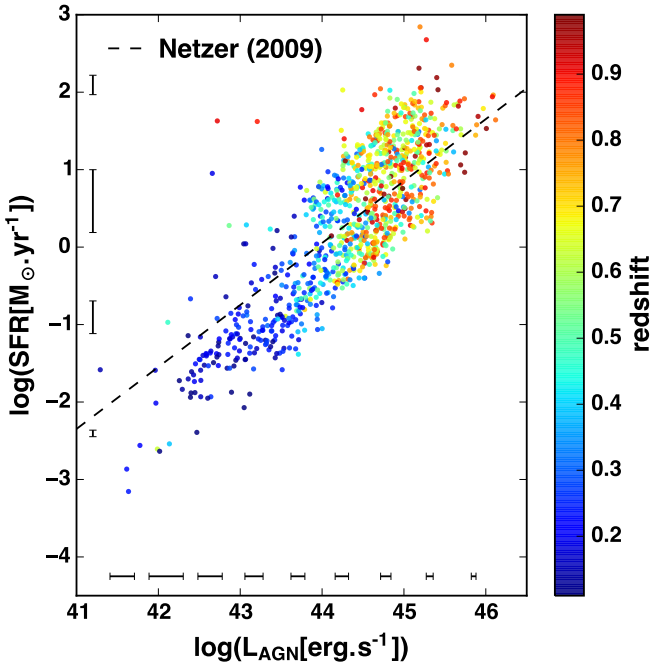

Figure 7. SFR-bolometric AGN luminosity. Points are color coded by the redshifts. Error bars show the median error in bins of SFR or $L_{\rm AGN}$..

and $L_{\rm AGN}$ we observe is preserved at all redshifts sampled here. We note that Stanley et al. (2015) use a different technique to determine the SFR, which is likely to yields overestimates in the case of Type 2 AGNs (Ciesla et al. 2015). We compare our results with the average SFR-$L_{\rm AGN}$ relation observed by Netzer (2009, dashed line on Fig. 7) from a sample at low redshift ($z \sim 0.1$) of Type I and Type II AGN. Netzer (2009) further shows that higher redshift ($z \sim 2-3$) QSOs from Lutz et al. (2008) also fall on this relation, at higher SFRs and $L_{\rm AGN}$. Our results are in excellent agreement with the relation from

Netzer (2009). We note that the object selection used by Netzer (2009) is different from the one we use as it combines Types I and II selected from spectral features in the restframe optical; moreover the methods Netzer (2009) used to derive SFR and $L_{\rm AGN}$ are completely different from ours.
We also checked that our SED fitting technique enables to probe the whole range of SFR and $L_{\rm AGN}$. In details, the models we use do probe the whole range; moreover the actual values of the parameters (SFR and $L_{\rm AGN}$) we use are derived from the PDF built during the SED fitting which also allows a larger spread around the models.
In a recent work, Rosario et al. (2012) studied the properties of X-ray selected AGN at $z < 2.5$ using constraints in the FIR from Herschel/PACS data. They found that at high $L_{\rm AGN}$ luminosities, the SFR-$L_{\rm AGN}$ relation follows a trend similar to the one we observe, but at lower luminosities, the average SFR is constant. Their findings are in line with the earlier results from Lutz et al. (2010) who performed stacking at 870 μm using similar AGN samples. These two regimes in the SFR-$L_{\rm AGN}$ relation are expected to reflect the two regimes of blak hole growth, starburst-like at high $L_{\rm AGN}$, and "hot halo" at low $L_{\rm AGN}$ (e.g. Gutcke et al. 2015). Our results do not support these observations. We note that Rosario et al. (2012) results are based on the luminosities at 60 μm, while we derive here a SFR from a full SED modelling. Rosario et al. (2012) argue that their 60 μm luminosity estimates are not contaminated by AGN emission. As mentioned by Rosario et al. (2012), AGN contribution to the SED at 60 μm would require large dust torii (Fritz et al. 2006), which are thought to be rare.
A potential reason for the difference between our results and those from Rosario et al. (2012) is that our selection does not bias against quiescent galaxies, or galaxies with very low star formation rates. Note that Salvato et al. (2009) showed that the fraction of quiescient galaxies in the XMM-Newton COSMOS sample (the catalog used by Rosario et al. (2012) in the COSMOS field) is small. Another possible reason for the discrepancy is that we do not probe well AGN fainter than $L_{\rm AGN} \lesssim 10^{42.5}$erg.s^{-1}, a range where Rosario et al. (2012) observe the flattening of the SFR-$L_{\rm AGN}$ relation. Our variability selection is also biased against fainter sources. Due to photometric errors, faint AGN require a larger fractional variability to be detected than bright AGN (see Sect. 4.3). Thus, this will translate to a luminosity threshold at a given redshift range below which we are unable to detect variability.

4.5. *AGN and the Main Sequence of Star Formation*

In Fig. 8 we show the location of AGN in the SFR-M_* plane, color-coded by the AGN bolometric luminosity, along with the distribution of galaxies in the control sample as contours. We also show the fit to the locus of the main sequence of star-forming galaxies obtained by Schreiber et al. (2015), at the median reshifts of the control sample ($z_{\rm median} = 0.39$), after converting their results to a Chabrier IMF.

A number of studies have extensively investigated the relation between SFR and M_* for inactive galaxies , from low to high redshifts (e.g. Elbaz et al. 2007; Noeske et al. 2007; Karim et al. 2011; Heinis et al. 2014; Schreiber et al. 2015). Our control sample clearly displays the star-forming sequence with a relation between SFR and M_* similar to the results obtained by Schreiber et al. (2015), while the bulk of quiescent galaxies are located at lower SFRs and relatively high M_* ($\sim 10^{10.75} M_\odot$). Above a stellar mass of $\sim 10^{9.5} M_\odot$, AGN occupy the full range of SFRs. The bolometric AGN luminosity is mostly correlated with SFR, with a weaker additional correlation with M_*.
Running a principal component analysis (PCA) on SFR, $L_{\rm AGN}$, and M_* shows that in this space, M_* encodes only 5% of the available information. While the distributions of AGN hosts and inactive galaxies look similar above $\sim 10^{9.5} M_\odot$, they are not strictly-speaking drawn from the same parent distribution, according to Kolmogorov-Smirnov and Mann-Whitney statistics. There is for instance virtually no AGN at $M_* > 10^{11.25} M_\odot$ and SFR$< 1 M_\odot$yr^{-1}.
We do observe however a significant fraction of AGN hosts within the main sequence of star forming galaxies. Assuming that the dispersion around the main sequence is 0.3 dex, we determine the percentages of AGN hosts that are above the main sequence, within the main sequence, or below the main sequence. We also perform the same for our control sample, mass matched this time. We derive errors on these fractions using the errors on the stellar mass and SFRs. The results are shown in Fig. 9. The percentages of AGN hosts and control sample galaxies show the same trend, that they decrease from quiescent to starburst. However, the percentage of AGN in quiescent hosts is significantly lower than for the control sample. On the other hand, the occurrence of AGN in MS or starburst hosts is larger than for the control sample. These results suggest that AGN activity is, at least moderately, linked to star formation activity.

5. DISCUSSION

5.1. *AGN variability*

We first note that our variable AGN sample has been selected from the PS1 transient alerts, which are by definition variable at the 5 σ level in at least 3 epochs in a time window of 15 days, properly measuring signal-to-noise in the individual difference images (see Sect. 2.1). This selection criteria does mean that fainter sources must have a larger fractional variability than brighter sources (see Sect. 4.3) to be detected at the 5 σ level. However, we find in our simulations that regardless of this bias, we are still capable of detecting AGN across the full range of host galaxy masses (see Fig. 3). Similarly, the trends shown in Fig. 5 and Fig. 6 cannot be attributed to this selection bias, since our sensitivity to variability at the low-luminosity end is well below the observed relations.

Our results on AGN variability are consistent with previous studies that showed that the variability amplitude decreases with AGN luminosity (Hook et al. 1994; Trevese et al. 1994; Vanden Berk et al. 2004; Wilhite et al. 2008; Bauer et al. 2009; Zuo et al. 2012; Gallastegui-Aizpun & Sarajedini 2014). This trend has been interpreted in the context of Poissonian models, where variations are due to the stochastic superposition of independent flares (e.g. Cid Fernandes et al. 2000). These models predict that the relation between variability amplitude and luminosity have a slope of -0.5. We do ob-

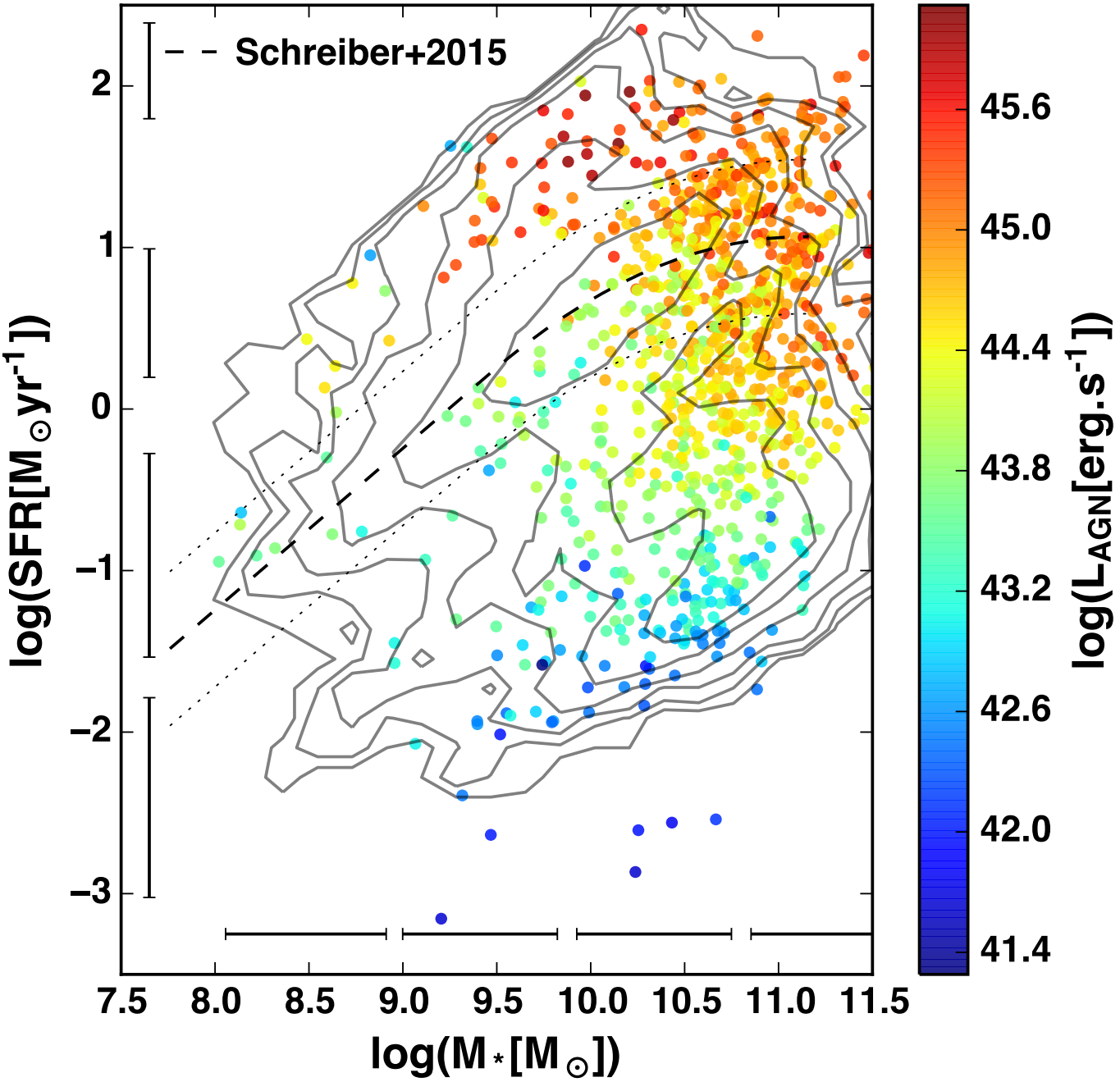

Figure 8. SFR-M_* relation. The gray contours show the relation for the control sample. The filled circles represent the AGN sample, color coded by $L_{\rm AGN}$. Error bars show the median error in bins of SFR or M_*. The dashed line shows the fit to the main sequence of star forming galaxies from Schreiber et al. (2015) at the median redshift of the sample. The dotted lines shows the limits we use for the main sequence, assuming a dispersion of 0.3 dex.

serve slopes consistent with this value, when we consider all objects in our sample, in the r, i, and z bands. The fact that we do not observe relations consistent with the Poissonian case does not actually rule it out. Indeed, selection effects might yield a not well defined variability relation, and moreover, a slope of -0.5 is only expected in the case of the simplest Poissonian models, where all the components of the models are universal constants among all objects (Cid Fernandes et al. 1996).

As previously noticed by Gallastegui-Aizpun & Sarajedini (2014), we observe that the relation between the variability and $L_{\rm AGN}$ steepens at redder wavelengths. A potential interpretation for this effect in a Poissonian context is that there is an underlying nonvariable background component redder than the SED of the flares (Cid Fernandes et al. 2000). We find however that this trend is luminosity dependent: for AGN with $L_{\rm AGN} \gtrsim 10^{43.5}\,{\rm erg.s^{-1}}$ our results show that the variability is larger in g, but for fainter AGN, the trend is reversed. In the context of accretion disk models (Shakura & Sunyaev 1976), where the variability is caused by a change in the accretion rate, one expects the variability to decrease monotonically with wavelength (e.g. Li & Cao 2008), which is inconsistent with our results at the faint end. While the "bluer when brighter" AGN are the most commonly observed, some "redder when brighter" AGN

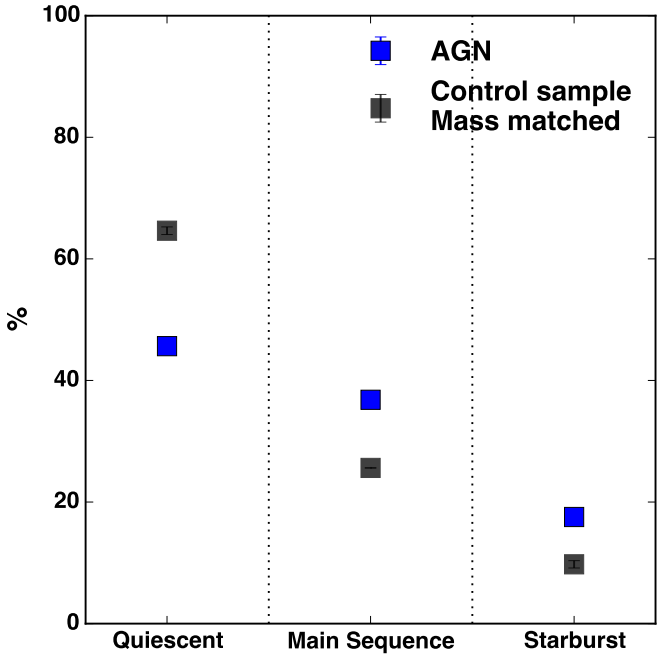

Figure 9. Percentage of AGN hosts (blue squares) below the main sequence, ('Quiescent'), on the main sequence, and above ('Starburst'). Percentages for the mass matched control sample are shown in black squares. Error bars on percentages are displayed, but are smaller than the size of the symbols.

have also been noticed. In particular, Gu et al. (2006) noticed using data spanning three months two flat spectrum radio quasars that become redder when brighter, which was confirmed by Rani et al. (2010). Gu et al. (2006) interpret this observation as the non-thermal component dominating the UV-optical region of the spectrum when the source brightens.

5.2. *AGN and host properties*

The link between AGN and their host properties has been widely studied over the last decades, using various techniques and selections. We revisit here this topic thanks to our variability selected AGN.

5.2.1. *Color distribution*

Our first result is that, after removing the contribution af the AGN to the observed color, we find that the color distribution of AGN hosts is similar to that of inactive galaxies. We note here that the reason the color distribution of our control sample is not bimodal comes from the fact that we are matching the mass and the i-band apparent magnitude distributions of the control galaxies to that of the AGNs. Our result that the color distribution of AGN hosts is similar to that of inactive galaxies is in contrast with a number of studies which observed that AGN are particularly common in green valley galaxies, suggesting that they are responsible for the quenching of star formation in this population: Martin et al. (2007) were one the first authors to make this observation; we however note that their $NUV - r$ was not corrected from AGN contamination. Schawinski et al. (2009) studied the host properties of a sample of X-ray selected AGNs, and subtracted a central point source in optical imaging to derive the host optical colors. They claimed that AGN are mostly found in green valley galaxies. We argue here that our results are actually consistent with theirs, once selection effects are taken into account. First of all, we note that Schawinski et al. (2009) observe few AGN in hosts fainter than $M_{\rm r} = -20.5$. This is in line with the fact that we observe very few AGN in host with stellar masses smaller than $M_* \sim 10^{9.5}\,M_\odot$. Within the range of $M_{\rm r}$ where their sample probes hosts bluer than the red sequence, the color distribution of AGN hosts is rather similar to what we observe. Moreover, the sample of Schawinski et al. (2009) is limited at $L_{0.1-2.4{\rm keV}} > 10^{42}\,{\rm ergs}^{-1}$, which corresponds to a bolometric luminosity of $L_{\rm AGN} \sim 10^{43}\,{\rm ergs}^{-1}$, assuming a bolometric correction of 10. Given the good correlation we observe between $L_{\rm AGN}$ and SFR (Fig. 7), this luminosity cut explains why Schawinski et al. (2009) do not observe any AGN within the red sequence. In this context, Xue et al. (2010) showed that it is essential to properly take into account selection effects to discuss the relation between AGN and host properties. They note in particular that it is critical to use mass-matched samples to compare the color distributions of AGN hosts and non-AGN galaxies. Once this is taken into account, they also found that these color distributions are similar, from $z = 3$ to $z = 0$. Aird et al. (2012) also found that the AGN fraction is only moderately enhanced in galaxies with blue or green colors.

5.2.2. *AGN-SFR connection*

A large number of studies have focused on the link between AGN and SFR activity, as AGN feedback has been shown in simulations to be a promising mechanism to quench star formation in galaxies, and explain the global trends in galaxy evolution since $z = 2$. Our point is not to contradict the fact that AGN *do* quench star formation in some galaxies. It is clear that AGN can inject in the intergalactic medium significant amounts of energy that can prevent further gas from cooling (Croton et al. 2006; Fabian 2012; Tombesi et al. 2015). However, the question is rather whether AGN feedback is statistically the main process that drives the building of the red sequence of galaxies observed since $z = 2$. Our results show that there is a good correlation between AGN and SFR over the whole ranges of redshift and bolometric luminosity we probed here, and hence that it is not obvious that AGN feedback is the dominant process. Our results for the SFR-$L_{\rm AGN}$ correlation are in contrast with the results from Lutz et al. (2008) and Rosario et al. (2012) who, based on X-ray AGN selected samples and stacking in the FIR, observe a plateau in the SFR-$L_{\rm AGN}$ relation for faint AGN. This can be interpreted (e.g. Gutcke et al. 2015) by two modes of AGN accretion. The mode corresponding to the SFR-$L_{\rm AGN}$ corrrelation is the "starburst" regime, where galaxies experience starburst and AGN activity with high SFR and black hole accretion rates. The other mode, corresponding to the plateau observed by Lutz et al. (2008) and Rosario et al. (2012), is the "hot-halo" regime, where the growth of the black holes is linked to the AGN feedback mechanism.
The discrepancy between the results of Lutz et al. (2008) and Rosario et al. (2012) and ours is mitigated by the fact that we do not probe well the range of luminosities where Lutz et al. (2008) and Rosario et al. (2012) observe the plateau ($L_{\rm AGN} \lesssim 10^{43}\,{\rm ergs}^{-1}$). However, the SFR values for the few objects we observe in that range are not

consistent with a plateau. One possibility is that our SED fitting procedure would erroneously mistake moderate levels of star formation for moderate levels of AGN activity. However, this seems unlikely according to the work of Ciesla et al. (2015), who showed that at low levels of AGN activity the SED procedure we use properly recovers the SFR. According to the simulations of Gutcke et al. (2015), the plateau in the SFR-$L_{\rm AGN}$ correlation is created by a mix of galaxies on and out of the main sequence. We note however that there are some discrepancies between these simulations and the observations. For instance the $z \sim 0$ results from Rosario et al. (2012) are based on the *Swift* BAT AGN sample of Cusumano et al. (2010). According to Koss et al. (2011), the minimum stellar mass for the hosts of this sample is around $M_* \sim 10^{9.8} M_\odot$. In this case it is unlikely, according to the simulations of Gutcke et al. (2015) that faint AGN with hosts more massive than this limit would have an average SFR larger than one (see their Fig. 5).
In summary, our results suggest that for $0 < z < 1$ there is a good correlation between AGN host SFR and $L_{\rm AGN}$. This implies that the black hole accretion rates are also well correlated with SFR. These results are consistent with the picture that AGN hosts experience secular evolution, and that black holes are mostly fueled by the same mechanisms that fuel star formation events. We visually inspected the objects in our sample with higher SFRs, and did not find any merger or interaction signatures. This does not mean that mergers or interactions do not trigger AGN activity, but rather it suggests that these events are not the main channels for AGN accretion. These results are in line with the results from Mullaney et al. (2012b) who found that the accretion rates of supermassive black holes are well correlated with SFR from $z = 2$ to $z = 1$. We note however that while our results are in line with previous ones suggesting that there is a good correlation between SFR and black hole activity, we can not get more insight from these results about the physical mechanisms at play in this correlation. Moreover, our sample is biased against Type 2 AGNs. Assuming the scenario of Hopkins et al. (2008) this means that we would be missing a fraction of the AGN population at stages where the star formation and AGN activity are still coexisting. This population of AGNs are hosted by ULIRGs type of objects, that we would miss with our UV/optical restframe selections.

6. CONCLUSIONS

We studied the properties of $\sim$ 1000 hosts of AGN at $z < 1$ selected by variability in optical bands in the Pan-STARRS1 survey. Thanks to extensive wavelength coverage from the UV to the FIR, we performed reliable AGN/host decomposition through SED fitting. Our results can be summarized as follows:

- We observe AGN in mostly in massive hosts: $M_* \gtrsim 10^{9.5}\, M_\odot$
- The relative amplitude of AGN variability decreases with AGN bolometric luminosity. This relation steepens with wavelength (between g and z band), and the steepening is driven by faint AGN $L_{\rm AGN} < 10^{43.5}\,{\rm ergs}^{-1}$.
- The $NUV - r_{\rm restframe}$ color distribution of AGN hosts is similar to a mass-matched control sample of non-AGN galaxies.
- We observe a well defined correlation between $L_{\rm AGN}$ and SFR, valid over the whole redshift range we probe, as well as for $10^{42.5} < L_{\rm AGN} < 10^{45.5}\,{\rm ergs}^{-1}$
- Above $M_* \gtrsim 10^{9.5}\, M_\odot$, AGN are most likely to be hosted by Main Sequence or starburst galaxies than by quiescent ones.
- These results suggest that there is no obvious correlation between AGN activity and SFR quenching at $z < 1$. This is in line with the results of a number of previous studies; however this study does not enable us to point towards a specific fueling mechanism.

It is a pleasure to thank Véronique Buat and Laure Ciesla for help with the `pCIGALE` software. We also thank Richard Mushotzky for stimulating discussions.

The Pan-STARRS1 Surveys (PS1) have been made possible through contributions of the Institute for Astronomy, the University of Hawaii, the Pan-STARRS Project Office, the Max-Planck Society and its participating institutes, the Max Planck Institute for Astronomy, Heidelberg and the Max Planck Institute for Extraterrestrial Physics, Garching, The Johns Hopkins University, Durham University, the University of Edinburgh, Queen's University Belfast, the Harvard-Smithsonian Center for Astrophysics, the Las Cumbres Observatory Global Telescope Network Incorporated, the National Central University of Taiwan, the Space Telescope Science Institute, the National Aeronautics and Space Administration under Grant No. NNX08AR22G issued through the Planetary Science Division of the NASA Science Mission Directorate, the National Science Foundation under Grant No. AST-1238877, the University of Maryland, and Eotvos Lorand University (ELTE) and the Los Alamos National Laboratory.

Funding for the DEEP2 Galaxy Redshift Survey has been provided in part by NSF grant AST00-71048 and NASA LTSA grant NNG04GC89G. Funding for PRIMUS is provided by NSF (AST-0607701, AST-0908246, AST-0908442, AST-0908354) and NASA (Spitzer-1356708, 08-ADP08-0019, NNX09AC95G). This paper uses data from the VIMOS Public Extragalactic Redshift Survey (VIPERS). VIPERS has been performed using the ESO Very Large Telescope, under the "Large Programme" 182.A-0886. The participating institutions and funding agencies are listed at http://vipers.inaf.it

REFERENCES

Aird, J., Coil, A. L., Moustakas, J., et al. 2012, ApJ, 746, 90
Alam, S., Albareti, F. D., Allende Prieto, C., et al. 2015, arXiv:1501.00963
Arnouts, S., Cristiani, S., Moscardini, L., et al. 1999, MNRAS, 310, 540
Bauer, A., Baltay, C., Coppi, P., et al. 2009, ApJ, 696, 1241
Bennert, N., Canalizo, G., Jungwiert, B., et al. 2008, ApJ, 677, 846

Bennert, V. N., Auger, M. W., Treu, T., Woo, J.-H., & Malkan, M. A. 2011, ApJ, 742, 107
Bertin, E., & Arnouts, S. 1996, A&AS, 117, 393
Bruzual, G., & Charlot, S. 2003, MNRAS, 344, 1000
Buat, V., Heinis, S., Boquien, M., et al. 2014, A&A, 561, A39
Budavári, T., Heinis, S., Szalay, A. S., et al. 2009, ApJ, 694, 1281
Calzetti, D., Armus, L., Bohlin, R. C., et al. 2000, ApJ, 533, 682
Canalizo, G., & Stockton, A. 2001, ApJ, 555, 719
Cardelli, J. A., Clayton, G. C., & Mathis, J. S. 1989, ApJ, 345, 245
Chabrier, G. 2003, PASP, 115, 763
Cid Fernandes, R., Jr., Aretxaga, I., & Terlevich, R. 1996, MNRAS, 282, 1191
Cid Fernandes, R., Sodré, L., Jr., & Vieira da Silva, L., Jr. 2000, ApJ, 544, 123
Ciesla, L., Charmandaris, V., Georgakakis, A., et al. 2015, A&A, 576, AA10
Cisternas, M., Jahnke, K., Inskip, K. J., et al. 2011, ApJ, 726, 57
Cohen, R. D., Puetter, R. C., Rudy, R. J., Ake, T. B., & Foltz, C. B. 1986, ApJ, 311, 135
Coil, A. L., Blanton, M. R., Burles, S. M., et al. 2011, ApJ, 741, 8
Cool, R. J., Moustakas, J., Blanton, M. R., et al. 2013, ApJ, 767, 118
Croton, D. J., Springel, V., White, S. D. M., et al. 2006, MNRAS, 365, 11
Cusumano, G., La Parola, V., Segreto, A., et al. 2010, A&A, 510, A48
Dale, D. A., Helou, G., Magdis, G. E., et al. 2014, ApJ, 784, 83
Denney, K. D., De Rosa, G., Croxall, K., et al. 2014, ApJ, 796, 134
Efstathiou, A., & Rowan-Robinson, M. 1995, MNRAS, 273, 649
Elbaz, D., Daddi, E., Le Borgne, D., et al. 2007, A&A, 468, 33
Fabian, A. C. 2012, ARA&A, 50, 455
Farrah, D., Urrutia, T., Lacy, M., et al. 2012, ApJ, 745, 178
Feltre, A., Hatziminaoglou, E., Fritz, J., & Franceschini, A. 2012, MNRAS, 426, 120
Fritz, J., Franceschini, A., & Hatziminaoglou, E. 2006, MNRAS, 366, 767
Gabor, J. M., Impey, C. D., Jahnke, K., et al. 2009, ApJ, 691, 705
Gallastegui-Aizpun, U., & Sarajedini, V. L. 2014, MNRAS, 444, 3078
Garilli, B., Le Fèvre, O., Guzzo, L., et al. 2008, A&A, 486, 683
Gezari, S., Martin, D. C., Forster, K., et al. 2013, ApJ, 766, 60
Gezari, S., Jones, D. O., Sanders, N. E., et al. 2015, ApJ, 804, 28
Gu, M. F., Lee, C.-U., Pak, S., Yim, H. S., & Fletcher, A. B. 2006, A&A, 450, 39
Gutcke, T. A., Fanidakis, N., Maccio', A. V., & Lacey, C. 2015, arXiv:1505.07245
Guzzo, L., Scodeggio, M., Garilli, B., et al. 2014, A&A, 566, AA108
Häring, N., & Rix, H.-W. 2004, ApJ, 604, L89
Hatziminaoglou, E., Fritz, J., Franceschini, A., et al. 2008, MNRAS, 386, 1252
Hatziminaoglou, E., Omont, A., Stevens, J. A., et al. 2010, A&A, 518, LL33
Heinis, S., Buat, V., Béthermin, M., et al. 2014, MNRAS, 437, 1268
Hopkins, P. F., Hernquist, L., Cox, T. J., & Kereš, D. 2008, ApJS, 175, 356
Hook, I. M., McMahon, R. G., Boyle, B. J., & Irwin, M. J. 1994, MNRAS, 268, 305
Ilbert, O., Arnouts, S., McCracken, H. J., et al. 2006, A&A, 457, 841
Ilbert, O., Capak, P., Salvato, M., et al. 2009, ApJ, 690, 1236
Ivezic, Z., Tyson, J. A., Abel, B., et al. 2008, arXiv:0805.2366
Kaiser, N., Burgett, W., Chambers, K., et al. 2010, Proc. SPIE, 7733, 77330E
Karim, A., Schinnerer, E., Martínez-Sansigre, A., et al. 2011, ApJ, 730, 61
Klesman, A. J., & Sarajedini, V. L. 2014, MNRAS, 442, 314
Kelly, B. C., Bechtold, J., & Siemiginowska, A. 2009, ApJ, 698, 895
Kelly, B. C., Vestergaard, M., Fan, X., et al. 2010, ApJ, 719, 1315
Kocevski, D. D., Faber, S. M., Mozena, M., et al. 2012, ApJ, 744, 148
Kormendy, J., & Ho, L. C. 2013, ARA&A, 51, 511
Koss, M., Mushotzky, R., Veilleux, S., et al. 2011, ApJ, 739, 57
Krawczyk, C. M., Richards, G. T., Mehta, S. S., et al. 2013, ApJS, 206, 4
Kumar, S., Gezari, S., Heinis, S., et al. 2015, ApJ, 802, 27
LaMassa, S. M., Cales, S., Moran, E. C., et al. 2015, ApJ, 800, 144
Lang, D. 2014, AJ, 147, 108
Lang, D., Hogg, D. W., & Schlegel, D. J. 2014, arXiv:1410.7397
Le Fèvre, O., Vettolani, G., Paltani, S., et al. 2004, A&A, 428, 1043
Le Fèvre, O., Vettolani, G., Garilli, B., et al. 2005, A&A, 439, 845
Li, S.-L., & Cao, X. 2008, MNRAS, 387, L41
Lilly, S. J., Le Fèvre, O., Renzini, A., et al. 2007, ApJS, 172, 70
Lutz, D., Sturm, E., Tacconi, L. J., et al. 2008, ApJ, 684, 853
Lutz, D., Mainieri, V., Rafferty, D., et al. 2010, ApJ, 712, 1287
Magnier, E. 2006, The Advanced Maui Optical and Space Surveillance Technologies Conference, 50
Magorrian, J., Tremaine, S., Richstone, D., et al. 1998, AJ, 115, 2285
Martin, D. C., Fanson, J., Schiminovich, D., et al. 2005, ApJ, 619, L1
Martin, D. C., Wyder, T. K., Schiminovich, D., et al. 2007, ApJS, 173, 342
MacLeod, C. L., Ivezić, Ž., Sesar, B., et al. 2012, ApJ, 753, 106
McConnell, N. J., & Ma, C.-P. 2013, ApJ, 764, 184
Mullaney, J. R., Pannella, M., Daddi, E., et al. 2012, MNRAS, 419, 95
Mullaney, J. R., Daddi, E., Béthermin, M., et al. 2012, ApJ, 753, L30
Netzer, H. 2009, MNRAS, 399, 1907
Netzer, H., & Trakhtenbrot, B. 2014, MNRAS, 438, 672
Newman, J. A., Cooper, M. C., Davis, M., et al. 2013, ApJS, 208, 5
Noeske, K. G., Weiner, B. J., Faber, S. M., et al. 2007, ApJ, 660, L43
Noll, S., Burgarella, D., Giovannoli, E., et al. 2009, A&A, 507, 1793
Page, M. J., Symeonidis, M., Vieira, J. D., et al. 2012, Nature, 485, 213
Rani, B., Gupta, A. C., Strigachev, A., et al. 2010, MNRAS, 404, 1992
Reines, A. E., & Volonteri, M. 2015, ApJ, 813, 82
Richards, G. T., Myers, A. D., Gray, A. G., et al. 2009, ApJS, 180, 67
Rosario, D. J., Santini, P., Lutz, D., et al. 2012, A&A, 545, A45
Rosario, D. J., Trakhtenbrot, B., Lutz, D., et al. 2013, A&A, 560, A72
Salvato, M., Hasinger, G., Ilbert, O., et al. 2009, ApJ, 690, 1250
Salvato, M., Ilbert, O., Hasinger, G., et al. 2011, ApJ, 742, 61
Sarajedini, V. L., Koo, D. C., Phillips, A. C., et al. 2006, ApJS, 166, 69
Schawinski, K., Virani, S., Simmons, B., et al. 2009, ApJ, 692, L19
Schlegel, D. J., Finkbeiner, D. P., & Davis, M. 1998, ApJ, 500, 525
Schmidt, K. B., Marshall, P. J., Rix, H.-W., et al. 2010, ApJ, 714, 1194
Schreiber, C., Pannella, M., Elbaz, D., et al. 2015, A&A, 575, A74
Seibert, M., Budavári, T., Rhee, J., et al. 2005, ApJ, 619, L23
Sesar, B., Ivezić, Ž., Lupton, R. H., et al. 2007, AJ, 134, 2236
Shakura, N. I., & Sunyaev, R. A. 1976, MNRAS, 175, 613
Shappee, B. J., Prieto, J. L., Grupe, D., et al. 2014, ApJ, 788, 48
Shen, Y., Richards, G. T., Strauss, M. A., et al. 2011, ApJS, 194, 45
Stanley, F., Harrison, C. M., Alexander, D. M., et al. 2015, arXiv:1502.07756
Stockton, A. 1982, ApJ, 257, 33
Szalay, A. S., Connolly, A. J., & Szokoly, G. P. 1999, AJ, 117, 68
Tohline, J. E., & Osterbrock, D. E. 1976, ApJ, 210, L117
Tombesi, F., Meléndez, M., Veilleux, S., et al. 2015, Nature, 519, 436
Treister, E., Schawinski, K., Urry, C. M., & Simmons, B. D. 2012, ApJ, 758, L39
Trevese, D., Kron, R. G., Majewski, S. R., Bershady, M. A., & Koo, D. C. 1994, ApJ, 433, 494
Vanden Berk, D. E., Wilhite, B. C., Kron, R. G., et al. 2004, ApJ, 601, 692
Véron-Cetty, M.-P., & Véron, P. 2010, A&A, 518, AA10

Villforth, C., Sarajedini, V., & Koekemoer, A. 2012, MNRAS, 426, 360
Wilhite, B. C., Brunner, R. J., Grier, C. J., Schneider, D. P., & vanden Berk, D. E. 2008, MNRAS, 383, 1232
Wyder, T. K., Martin, D. C., Schiminovich, D., et al. 2007, ApJS, 173, 293
Xue, Y. Q., Brandt, W. N., Luo, B., et al. 2010, ApJ, 720, 368
Zuo, W., Wu, X.-B., Liu, Y.-Q., & Jiao, C.-L. 2012, ApJ, 758, 104